

Use of Reverberation Chamber to Simulate the Power Delay Profile of a Wireless Environment

E. Genender^(1,2), C.L. Holloway⁽²⁾, K.A. Remley⁽²⁾, J. Ladbury⁽²⁾, G. Koepke⁽²⁾ and H. Garbe⁽¹⁾

(1)Leibniz University of Hannover, Institut fuer Grundlagen der Elektrotechnik und Messtechnik, Appelstrasse 9A, 30167 Hannover, Germany

(2)National Institute of Standards and Technology (NIST), 325 Broadway, Boulder, CO 80305, USA

Abstract—Multipath propagation environment effects, such as frequency-selective fading, have a strong impact on the quality of a wireless channel. For example, multipath can impact bit error rate (BER) differently from Gaussian noise. For testing wireless devices/systems in these multipath environments it is imperative to have a reliable, controllable, and statistically repeatable measurement facility. The purpose of this paper is to illustrate how the reverberation chamber can be used to simulate different multipath propagation environments. Channel characteristics such as power-delay profile, RMS-delay spread, and the Rician K -factor are examined. Results for different chamber configurations (e.g., loading of the chamber, antenna positions, etc.) are compared and their effects discussed. Results achieved inside a chamber are compared with those obtained in an actual industrial environment.

Keywords: delay spread, multipath propagation, power delay profile, reverberation chamber, Rician K -factor, wireless communications, wireless environment

I. INTRODUCTION

In recent years, wireless applications have increased in importance and are now used in many different types of environments from urban to indoor (e.g., homes, offices, factories, and aircrafts). Manufacturers of wireless systems want to be able to design and test these devices for use in any type of environment. Thus, it is essential to have a reliable and controllable facility where wireless devices can be tested. For that purpose an electromagnetic reverberation chamber is a potential test facility.

The reverberation chamber is essentially an electrically large metallic box. Inside the chamber, a metallic paddle (stirrer) is rotated, randomizing the electric field inside. The reverberation chamber is currently used for a wide range of wireless measurements [1-9]. It has already been shown that it is possible to manipulate the Rician K -factor, which describes the proportion of direct to scattered component of the electric field, in order to simulate different wireless environments [1]. The purpose of this

paper is to extend this work by looking at another important aspect of wireless channels: the power delay profile.

II. WIRELESS ENVIROMENT CHARACTERIZATION

A wireless channel can be described by its impulse response. For any fixed location between transmitter and receiver, under static conditions, the channel will have a linear impulse response $h(t)$. The output $y(t)$ of a static radio channel at time t can be calculated by

$$y(t) = u(t) * h(t) = \int_{-\infty}^{\infty} h(\tau) u(t - \tau) d\tau, \quad (1)$$

where $u(t)$ is the input time signal. To include the effects due to time and/or spatial varying multipath, we carry out an ensemble average. The ensemble average of the magnitude squared of the impulse response is referred to as the power delay profile (PDP) and is given by

$$PDP(t) = \langle |h(t)|^2 \rangle. \quad (2)$$

Different types of radio propagation environments produce differently shaped PDPs. For example, Figure 1 shows the PDP measured in an industrial environment (an oil refinery in Denver, Colorado).

The shape of the PDP can have adverse effects on the performance of digital communication systems. One characteristic of the PDP that has been shown to be particularly important in digital systems is the root-mean-square (RMS) delay spread of the PDP (which is basically the second central moment of the PDP) given by

$$\tau_{RMS} = \sqrt{\frac{\int (t - \tau_{ave})^2 PDP(t) dt}{\int PDP(t) dt}}, \quad (3)$$

where τ_{ave} is the average delay given by

$$\tau_{ave} = \frac{\int t PDP(t) dt}{\int PDP(t) dt} \quad (4)$$

RMS delay spread (τ_{RMS}) is often used to characterize a wireless communication environment because it is related to the BER performance of a channel [10, 11]. In fact, Chuang [10] has shown that, for certain digitally modulated signals, independent of the modulation scheme used, the BER is proportional to the quantity $(\tau_{RMS} T^{-1})^2$, where T is the bit period. The proportionality constant depends on the type of modulation. Simply, large values of τ_{RMS} compared to T lead to larger BER.

In designing communication systems, it is important to test the system in an environment (defined by the PDP and τ_{RMS}) similar to where it may be employed. Thus, a repeatable control test facility is needed. This paper describes how a reverberation chamber may be used as such a facility. We show that the PDP in the reverberation chamber can be controlled and how the τ_{RMS} can be manipulated to many desirable values. It is then possible to achieve a range of desirable radio environments for testing products. The results will be compared to measurements done in real multipath environments.

III. CONTROLLING RMS DELAY SPREAD

We carried out measurements of a simulated wireless environment using the setup shown in Figure 2. The test chamber was the NIST reverberation chamber, having the dimensions of 3.05 m \times 4.57 m \times 2.74 m. In order to control the τ_{RMS} of the chamber, the ring-down time, essentially the PDP , of the chamber needed to be controlled. Related to ring-down time is the quality factor Q , which is the proportion of energy stored to the energy dissipated per cycle:

$$Q = \frac{\omega U}{P}, \quad (5)$$

where ω is the radian frequency, U is the energy stored in the cavity, and P is the dissipated power. For a given reverberation chamber, the losses resulting from the finite conductivity of cavity walls, apertures and the loads in the antennas cannot be modified. However, we can change the loading of the chamber; i.e., by putting different numbers of blocks of absorbing material inside the chamber. This reduces the ring-down time, allowing us to match the τ_{RMS} in the chamber to a real radio-propagation environment.

Figure 3 shows the absorber used in the experiment. In these tests we used as many as seven pieces of identical absorbers. There is typically no need to increase the ring-down time since the unloaded chamber has much larger delay spreads than most real

applications. The exception to this would be metallic structures such as airplanes, metal enclosures, and buildings. Care has to be taken, because the chamber should not be loaded too much or statistical field uniformity will be destroyed [12].

In order to illustrate the change in Q for different loading, measurements were performed with different amounts of absorber. Two double ridge horn antennas were placed inside the chamber and connected to a vector network analyzer outside. The scattering parameter S_{21} was measured for several paddle positions, and Q was determined with this quantity [13]. Figure 4 shows the Q -factor depending on the number of pieces of absorbers used (zero, one, three and seven pieces).

To measure the impulse response of the reverberation chamber, we again used the two double ridge horn antennas and a vector network analyzer. The scattering parameter S_{21} was measured over a certain bandwidth and the Inverse Discrete Fourier Transformation (IDFT) was applied. This results in one impulse response. This was repeated for different paddle positions. The results were squared and averaged to obtain the PDP (as described in (2)). After that the PDP was normalized to its maximum power.

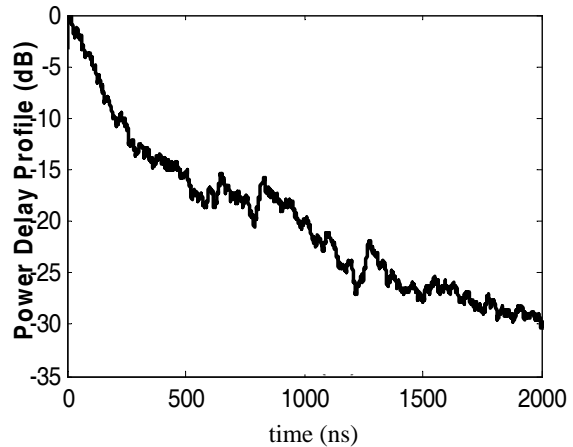


Figure 1. Example for a measurement PDP obtained in an industrial environment (an oil refinery in Denver, Colorado).

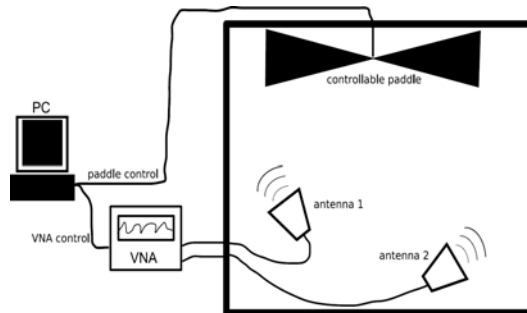


Figure 2. Illustration of the reverberation chamber setup.

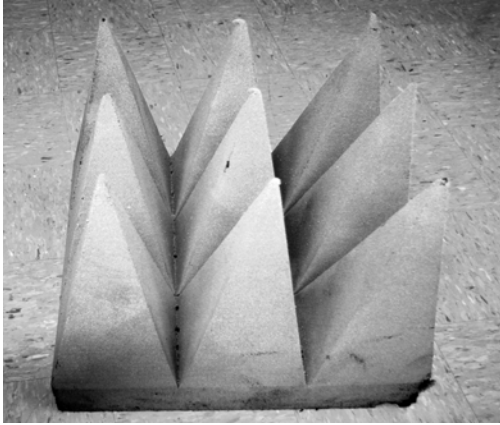


Figure 3. Absorber used in our measurements.

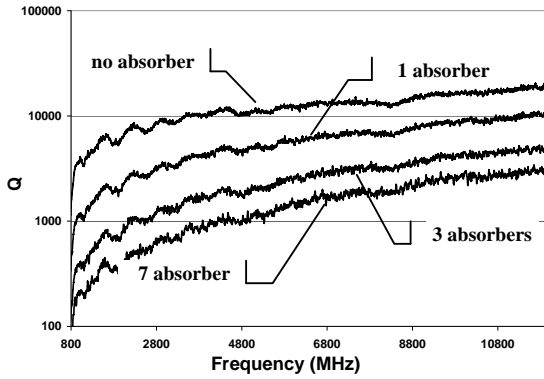


Figure 4. Q -factor measured for different numbers of absorbers inside the chamber as a function of frequency.

The results for zero, one, three, and seven pieces of absorber can be viewed in Figure 5. Which shows clearly the difference in decay for different loadings. For seven absorbers the noise floor is already reached after 1000 ns.

Because of the noise present in all measurements, τ_{RMS} cannot be calculated from the entire time record. Thus, the calculation has to be bounded to a certain threshold. We define the threshold as the minimum signal level beyond which the data are not taken into account when calculating τ_{RMS} . (The threshold is relative to the maximum signal value in a given measurement.) The point here is that when the noise floor is encountered, the resulting τ_{RMS} would be larger and larger as more and more of the time record is used in the calculation. However, we also need to use long time records to obtain the correct value of τ_{RMS} . Thus, we should expect that as we increase the maximum time record used in determining τ_{RMS} , the calculated τ_{RMS} should asymptotically approach the correct value until the noise floor is encountered, at

which point τ_{RMS} would increase over the correct value.

In order to illustrate the dependence of RMS delay spread on the threshold level, we have calculated τ_{RMS} for different threshold values, see Figure 6. This figure shows τ_{RMS} as a function of the threshold relative to the maximum value of the PDP . Depending on number of absorbers, thresholds below 20 dB to 30 dB achieve the final value without running into the noise floor. This shows that a threshold of about 30 dB can be used to obtain a reliable result. The results for the delay spread calculated with a threshold of 30 dB are shown in Figure 7. In order to compare τ_{RMS} for different loading, care needs to be taken in choosing a consistent threshold level for all loading.

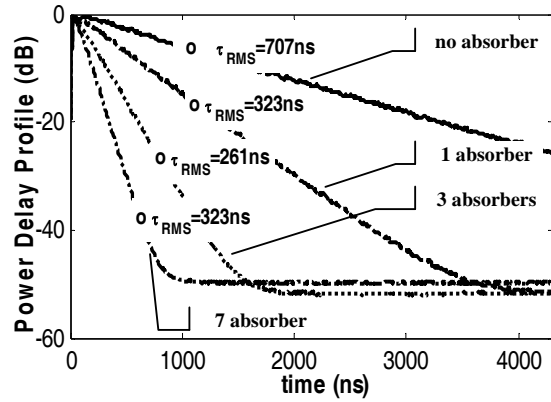


Figure 5. Power Delay Profile with the corresponding RMS delay spread measured for different numbers of absorbers.

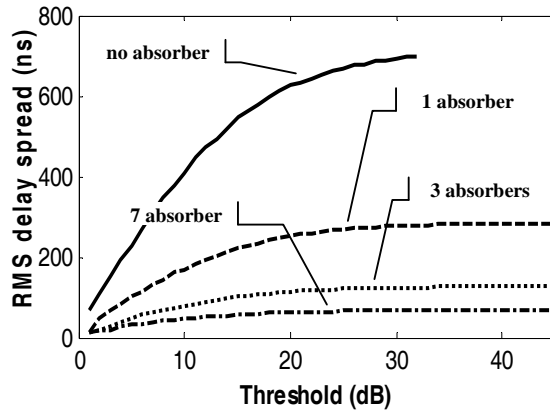


Figure 6. RMS delay spread calculated depending on the threshold relative to the maximum value of the Power Delay Profile.

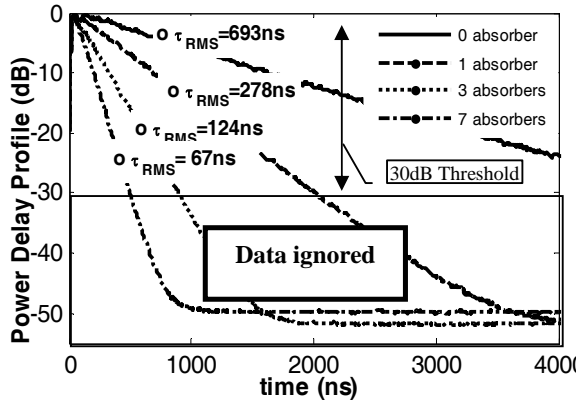


Figure 7. Power Delay Profile measured for different numbers of absorbers. The RMS delay spread is calculated with a 30 dB threshold.

In Figure 4 we saw that the Q -factor was dependent on the frequency. From this, we assume that the RMS delay spread could also be dependent on the frequencies used to obtain a time-domain representation of the measured signal. In the results above for PDP and τ_{RMS} , we used S_{21} obtained from measurements over a frequency range of 500 MHz to 12 GHz. One way to look at this is that using a wide frequency range (500 MHz-12 GHz) produces results that are a combination of different delay spreads. Most communications systems have a defined bandwidth of frequencies, usually much smaller than the 500 MHz to 12 GHz bandwidth used above.

In order to analyze the behavior of PDP and τ_{RMS} for a given center frequency and bandwidth, we used a 200 MHz band-pass filter in post-processing. This filter was applied to the S_{21} frequency-domain data, and the PDP s and τ_{RMS} were calculated for different filter center frequencies. The resultant PDP s for a few center frequencies are shown in Figure 8. The results in this figure are for one piece of absorber. Notice that the noise level differs for different center frequencies. Over 30 dB of difference is observed when comparing center frequencies of 1 GHz and 11 GHz.

The difference in decay and hence in the delay spread is now obvious in this figure. We next examined the behavior of RMS delay spread as function of frequency for the 200 MHz filter. For that, we swept the center frequency of the filter over the whole bandwidth and calculated τ_{RMS} . This was repeated for different numbers of absorbers. The results are shown in Figure 9. Figure 9 shows that for zero or one absorber, τ_{RMS} is strongly frequency dependent, while for three or seven absorbers, τ_{RMS} doesn't change significantly. The reason for this is that for small numbers of absorbers the wall loss dominates, and this effect has a particular frequency dependence. With more absorbers, the absorber begins to dominate the loss inside the chamber. Since the absorption losses of the absorber in the reverberation chamber behave

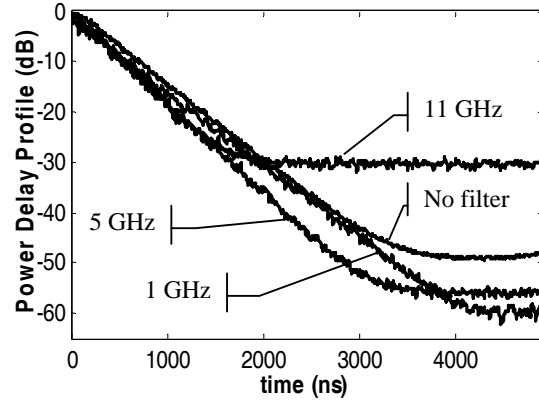


Figure 8. Power Delay Profile calculated for different center frequencies of a filter.

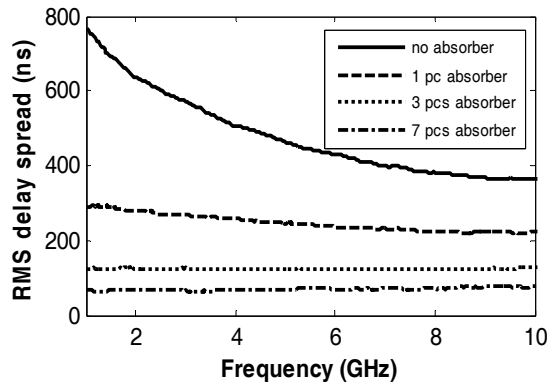


Figure 9. RMS delay spread measured for different numbers of absorbers, calculated for swept filter center frequency.

differently from the metallic wall, the absorption due to the absorber alone has different frequency dependence as compared to the metallic wall loss case. As a result, τ_{RMS} is fairly constant over frequency when metal wall losses are not dominant.

Another interesting way of looking at the data is to look at τ_{RMS} as a function of chamber Q -factor as a result of loading for a given frequency. Figure 10 shows the RMS delay spread as a function of the Q -factor for different frequencies.

The results show that the RMS delay spread is proportional to the chamber Q -factor for a given frequency. This result is significant because the Q -factor indicates how well the energy is kept inside the chamber.

Using this graph, the manufacturers of wireless devices could achieve a certain delay spread in any reverberation chamber for plotted frequencies just by adjusting the chamber Q -factor.

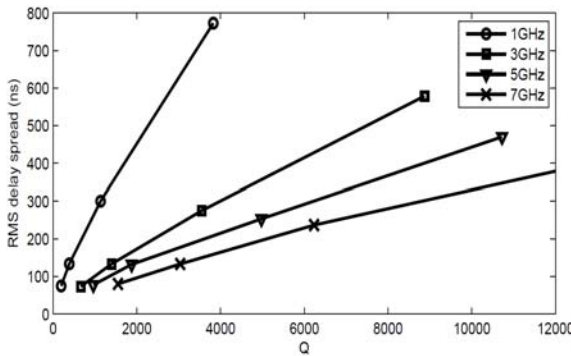


Figure 10. PDP measured for antennas pointing either at each other or into the corners of the chamber.

We have shown that τ_{RMS} can be controlled by changing the Q -factor of the chamber. These measurements were done for both antennas pointing at the corners, such that little direct, line-of-sight path was present. It is also possible to change the PDP inside a chamber by changing the Rician K -factor [1], which describes the ratio between the direct and scattered component of the energy inside the chamber.

Figure 11 shows the PDP measured for antennas pointing at different corners in the chamber and antennas pointing at each other. In the second case, a high peak value at about 10 ns is caused by the line-of-sight component. The offset of the two graphs in the figure is a result of the fact that both graphs are normalized to their maximum; hence the graph with the high peak is pushed down. Although the Q -factor for both experiments is the same, the RMS delay spread τ_{RMS} is different (for no direct coupling $\tau_{RMS}=69$ ns, for direct coupling $\tau_{RMS}=41$ ns). In the second case, the direct component is used in the calculation of τ_{RMS} . Hence, it is possible to manipulate the τ_{RMS} without changing the Q -factor. So using these two quantities, Q -factor and Rician K -factor, it is possible to create numerous types of the wireless environments inside the chamber.

In order to illustrate the ability of the reverberation chamber to simulate a realistic radio propagation environment, we compare the PDP measured in the chamber for different loading to the PDP measured in a factory (an oil refinery in Denver, Colorado). The comparison is plotted in Figure 12. The oil refinery consisted of several acres of piping and ductwork overhead and around the measurement set up. The high level of multipath arising from this propagation environment can make radio communication difficult. Simulating this and other industrial environments in the reverberation chamber can enable improved standards and designs of wireless devices. This comparison shows that an industrial environment can be simulated inside the chamber by adjusting the loading of the chamber.

IV. CONCLUSION

This paper has shown how the power delay profile and RMS delay spread can be measured and controlled inside a reverberation chamber. It was shown that changing the loading or the antenna direction influences τ_{RMS} . Experimental data were presented showing the relation between τ_{RMS} and the chamber Q -factor. The results were compared to data for a realistic radio environment; there it was shown that the reverberation chamber could simulate the realistic environment.

This paper presented experimental evidence showing that the reverberation chamber can be used to create various wireless propagation environments in order to test different wireless devices. In future work we will examine the behavior of the BER for different modulation types, different symbol durations and different carrier frequencies, for different chamber loadings.

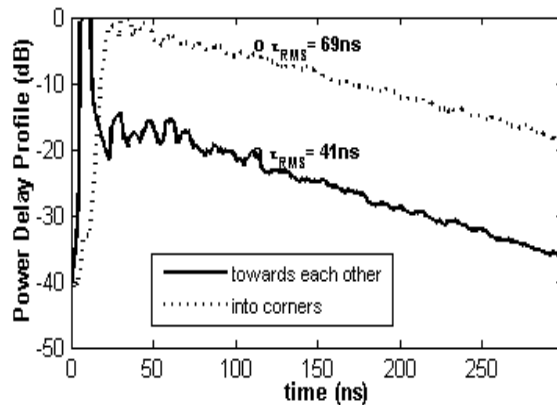


Figure 11. PDP measured for antennas pointing either at each other or into the corners of the chamber.

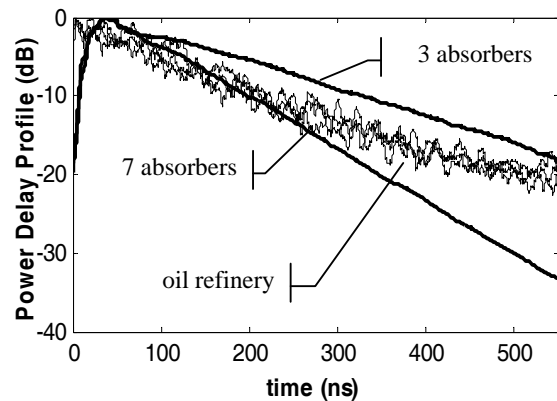


Figure 12. Comparison of measurements performed inside the NIST reverberation chamber to those made in a oil refinery.

ACKNOWLEDGEMENTS

The author thanks D. Camell and C. Grosvenor of NIST for providing the measured PDP data of the factory.

REFERENCES

- [1] C.L. Holloway, et. al., "On the use of reverberation chambers to simulate a controllable rician radio environment for the Testing of Wireless Devices", IEEE Transactions on Antennas and Propagation, vol. 54, no. 11, pp. 3167-3177, Nov. 2006.
- [2] N. Serafimov, et. al., "Comparison between radiation efficiencies of phone antennas and radiated power of mobile phones measured in anechoic chambers and reverberation chambers," in Proc. of the IEEE Antennas and Propagation International Symposium 2002, vol. 2, 478-481, June 2002.
- [3] P-S. Kildal, et. al., "Definition of effective diversity gain and how to measure it in a reverberation chamber," Microwave and Optical Technology Letters, vol. 34, no. 1, pp. 56-59, July 2002.
- [4] P.-S. Kildal, et. al., "Electromagnetic analysis of effective and apparent diversity gain of two parallel dipoles," IEEE Antennas and Wireless Propagation Letters, vol. 2, pp. 9-13, 2003.
- [5] P-S. Kildal, et. al., "Correlation and capacity of MIMO systems and mutual coupling, radiation efficiency, and diversity gain of their antennas: simulations and measurements in a reverberation chamber," IEEE Commun. Mag., vol. 42, no. 12, pp. 104-112, Dec. 2004.
- [6] M. Lienard, et. al., "Simulation of dual array multipath channels using mode-stirred reverberation chambers," Electronics Letters, vol. 40, no. 10, 578-579, May 2004.
- [7] M. Otterskog, et. al., "On creating a nonisotropic propagation environment inside a scattered field chamber," Microwave and Optical Technology Letters, vol. 43, no. 3, pp. 192-195, Nov., 2004.
- [8] C. Orlenius, et. al., "Measurements of total isotropic sensitivity and average fading sensitivity of CDMA phones in reverberation chamber," in the Proc. of IEEE AP-S International Symp., Washington D.C., 3-8 July 2005, vol 1A, pp. 409-412.
- [9] G. Ferrara, et. al., "Characterization of GSM non-line-of-sight propagation channels generated in a reverberating chamber by using bit error rates", IEEE Transactions on Electromagnetic Compatibility, vol. 49, no. 3, pp. 467-473, Aug. 2007.
- [10] J. Chuang., "The effects of time delay spread on portable radio communications channels with Digital Modulation," IEEE J. Selective Area on Cumm., vol 5, no. 5, pp. 879- 889, June, 1987.
- [11] S.R. Saunders, Antennas and Propagation for Wireless Communication Systems, 2nd Ed. John Wiley & Sons, 2007, p 245.
- [12] C.L. Holloway, et. al., "Requirements for an effective reverberation chamber: unloaded or loaded", IEEE Transactions on Electromagnetic Compatability, vol. 48, no. 1, Feb. 2006, pp. 187-194.
- [13] D. Hill, et. al., "Aperture excitation of electrically large, lossy cavities", IEEE Transactions on Electromagnetic Compatability, vol. 36, no. 3, Aug. 1994.